Journal of
Materials Chemistry C

ROYAL SOCIETY OF CHEMISTRY

PAPER

View Article Online
View Journal | View Issue

Cite this: J. Mater. Chem. C, 2018, 6, 4177

High performance Al_3Sc alloy doped Al_3Sc–Sb_2Te chalcogenides for phase change memory application

Sifan Zhang,[ac] Liangcai Wu,*[ab] Wenxiong Song,[a] Xilin Zhou,[d] Zhitang Song,[a] Jianjun Shi,[b] Jing Zhang[b] and Songlin Feng[a]

Published on 09 March 2018. Downloaded on 24/04/2018 12:51:46.

Received 3rd February 2018, Accepted 7th March 2018

DOI: 10.1039/c8tc00590g

rsc.li/materials-c

An Al_3Sc alloy doped Al_3Sc–Sb_2Te chalcogenide was put forward to avoid oxidation of pure Sc and enhance data retention ability. Compared with conventional $Ge_2Sb_2Te_5$ and Sc-doped $Sc_{0.2}Sb_2Te_3$ materials, the Al_3Sc alloy doped Al_3Sc–Sb_2Te chalcogenide has much better thermal stability and data retention. X-ray diffraction and transmission electron microscopy analysis reveal that the structure of Al_3Sc–Sb_2Te has no obvious change compared with Sb_2Te, except for the refined grain size. The Al_3Sc–Sb_2Te based device shows excellent reversible SET–RESET properties with a suitable operation window and a low power consumption of 1.38×10^{-11} J. In addition, a good cyclability of 1×10^6 cycles can be obtained with a large resistance ratio of about 10^2. Our calculations reveal that Al and Sc atoms prefer bonding with Te atoms. These stable local patterns stabilize glassy states and result in high stability.

1. Introduction

In recent years, along with rapid development of nonvolatile memories, phase change memory (PCM) has been considered as one of the most promising candidates for next generation non-volatile memory due to its excellent properties of logic compatibility, a scaling-favorable operation scheme, low fabrication cost, excellent scalability and high endurance.[1–6] It utilizes the resistance difference between the amorphous states (RESET state with high electrical resistivity) and crystalline states (SET state with low electrical resistivity) of chalcogenide phase change materials to encode digital information.[7–10] The amorphous film can be heated to the crystalline state by applying a longer but lower current pulse. In order to obtain the amorphous state, a shorter but higher current pulse is required to heat the film above the melting temperature.[11–15] $Ge_2Sb_2Te_5$ (GST) is the most widely used phase change material in PCM devices because GST-based PCM devices have been mass-produced. However, it also faces the problems of poor thermal stability and slow switching speed. Many studies have focused on doping Sb–Te alloys, such as Ti–Sb–Te[16,17] and $Sc_{0.2}Sb_2Te_3$,[18] and their good performance has been demonstrated. For example, the $Sc_{0.2}Sb_2Te_3$ compound allows a writing speed of 700 picoseconds without preprogramming. However, 10-year data retention temperature of the $Sc_{0.2}Sb_2Te_3$ compound is only 87 °C,[18] just a little higher than that of GST (about 85 °C).[19] Furthermore, due to the easy oxidation of the pure Sc target,[20,21] it is hard for practical application and hard for process control to utilize pure Sc target sputtering to fabricate devices.

Here, the Al_3Sc–Sb_2Te alloy material was put forward and the Al_3Sc alloy target was used to avoid the oxidation of Sc, and at the same time, to refine grain size and form smaller and uniform crystalline grains, which is important to improve the thermal stability and data retention of the amorphous state, reduce residual stress and enhance the stability of the PCM device. So Al_3Sc alloy doping is a viable alternative technical measure to prepare a highly thermally stable and fast switching Al_3Sc–Sb_2Te film. The Al_3Sc–Sb_2Te alloy material has much better data retention (10-year data retention temperature is 107 °C) than conventional $Ge_2Sb_2Te_5$ and recently reported $Sc_{0.2}Sb_2Te_3$ phase change materials.[18] The Al_3Sc–Sb_2Te based device shows excellent reversible SET–RESET properties with a good resistance ratio and an operation window. Furthermore, 1×10^6 cycles were demonstrated with a large resistance ratio of about 10^2. Calculations reveal that Al and Sc atoms prefer bonding with Te atoms. These stable local patterns stabilize the glassy states and result in high thermal stability.

2. Experimental and calculation

The Al_3Sc alloy doped Al_3Sc–Sb_2Te films with a thickness of 100 nm were deposited on SiO_2/Si(100) substrates by magnetron co-sputtering using separate Al_3Sc alloys and Sb_2Te targets at room temperature. The composition of the designed films was controlled by sputtering power and measured by energy

[a] State Key Laboratory of Functional Materials for Informatics, Shanghai Institute of Micro-system and Information Technology, Chinese Academy of Sciences, 200050 Shanghai, China. E-mail: wuliangcai@mail.sim.ac.cn
[b] College of Science, Donghua University, Shanghai 201620, China. E-mail: lcwu@dhu.edu.cn
[c] University of the Chinese Academy of Sciences, Beijing 100049, China
[d] Max Planck Institute of Microstructure Physics, Halle (Saale) D-06120, Germany

This journal is © The Royal Society of Chemistry 2018

Published on 09 March 2018. Downloaded on 24/04/2018 12:51:46.

dispersive spectroscopy. The Sb_2Te and $Sb_2Te(Al_3Sc)$-x (x = 1, 2, 3) films are used to denote undoped and Al_3Sc alloy doped Al_3Sc–Sb_2Te films, respectively. The resistance by a function of the temperature (R–T) was performed in a vacuum chamber with the heating rate of 20 °C min^{-1}. The density changes of 40 nm films before and after crystallization were studied by X-ray reflectivity (XRR) experiments (Bruker D8 Discover). X-ray diffraction (XRD) was adopted to characterize the lattice information of films. Then the microstructure was explored by Transmission Electron Microscopy (TEM) and High Resolution Transmission Electron Microscopy (HRTEM). Finally, Al_3Sc–Sb_2Te based "T-shaped" cells were fabricated to estimate the electrical performance of devices. Pre-technology was provided industrially by 0.13 mm CMOS technology. An 80 nm-thick phase change material and 10 nm-thick TiN as an adhesion layer were deposited using the sputtering method over a tungsten heating electrode of 190 nm diameter. The current–voltage (I–V), resistance–voltage (R–V), and endurance tests were carried out using a Tektronix AWG5002B arbitrary waveform generator and a Keithley 2400 m parameter analyzer.

Ab initio molecular-dynamics (AIMD) simulations of Al_3Sc–Sb_2Te were carried out based on density functional theory (DFT). The Kohn–Sham equations were solved using the Vienna *Ab Initio* Simulation package (VASP),[22–25] in which a single Γ point was used. The valence electron and core interactions were described using the projector augmented wave (PAW) method.[26] Electron exchange and correlation were described using the Perdew–Burke–Ernzerhof with van der Waals correction (PBE-D3) generalized gradient approximation (GGA) functional with a kinetic energy cutoff of 300 eV.[27] A model of 101 atoms was first melted at 3000 K for 20 ps with a time step Δt = 2 fs, and then it was relaxed at 800 K for 40 ps. In the simulations, the *NVT* ensemble of constant number, volume, and temperature was used, in which the temperature was regulated using a Nosé–Hoover thermostat.

3. Results and discussion

A temperature dependent resistance characteristic reflects the resistance change of phase change materials with heating temperature. The R–T curves of Sb_2Te and $Sb_2Te(Al_3Sc)x$ (x = 1, 2, 3) films were obtained at a heating rate of 20 °C min^{-1}. The results are shown in Fig. 1(a). With the increase of annealing temperature, the resistance decreases slowly at first, and then rapidly drops at crystallization temperature (T_c). The T_c is determined by minimum of the first derivative of the R–T curve. For the Sb_2Te film, T_c is estimated to be 148 °C. With the increase of the Al_3Sc doping amount, the T_c of $Sb_2Te(Al_3Sc)$-1, $Sb_2Te(Al_3Sc)$-2 and $Sb_2Te(Al_3Sc)$-3 gradually increase to 156 °C, 180 °C and 189 °C respectively. The increase of T_c indicates that the thermal stability of the amorphous state is improved. After doping Al_3Sc, the crystalline resistance also increases, helping in reducing the RESET current of the PCM device. The 10-year data retention of the $Sb_2Te(Al_3Sc)$-3 film is estimated by the extrapolation of the isothermal Arrhenius plots. Fig. 1(b) shows the fitting curve of log failure time to $1/k_BT$, which follows a linear relationship based on the Arrhenius equation: $t = \tau\exp(E_a/k_BT)$, where t, τ, E_a and k_B represent failure time, the proportional time coefficient, crystallization activation energy and Boltzmann's constant.[28] From the fitting curve, 10-year-data-retention temperatures are calculated to be 56 °C for Sb_2Te, 68 °C for $Sb_2Te(Al_3Sc)$-1, 79 °C for $Sb_2Te(Al_3Sc)$-2 and 107 °C for $Sb_2Te(Al_3Sc)$-3. And the activation energies of crystallization (E_a) are calculated to be 2.07 eV for Sb_2Te, 2.28 eV for $Sb_2Te(Al_3Sc)$-1, 2.29 eV for $Sb_2Te(Al_3Sc)$-2 and 3.08 eV for $Sb_2Te(Al_3Sc)$-3. The enhancement on data retention can be attributed to a higher T_c of Al_3Sc alloy doped Al_3Sc–Sb_2Te films. Compared with conventional GST and $Sc_{0.2}Sb_2Te_3$, $Sb_2Te(Al_3Sc)$-3 has a higher crystallization temperature and longer data retention, showing a much better thermal stability.

The change in the film density between amorphous and crystalline states is important for the PCM device performance. The density change of the $Sb_2Te(Al_3Sc)$-3 film was studied by the XRR technique. The crystalline $Sb_2Te(Al_3Sc)$-3 film was annealed at 230 °C for 3 min in a N_2 atmosphere. Amorphous and crystalline XRR patterns of $Sb_2Te(Al_3Sc)$-3 films are shown in Fig. 2(a), the y-axis shows the relative intensity and if the interface is smooth and sharp, then the reflected intensity of X-rays obeys the law of Fresnel reflectivity. Therefore, by analyzing the reflection intensity of different states, the information of films' thickness, density and roughness can be obtained. Fig. 2(b) depicts the thickness fit curve of $Sb_2Te(Al_3Sc)$-3 films before

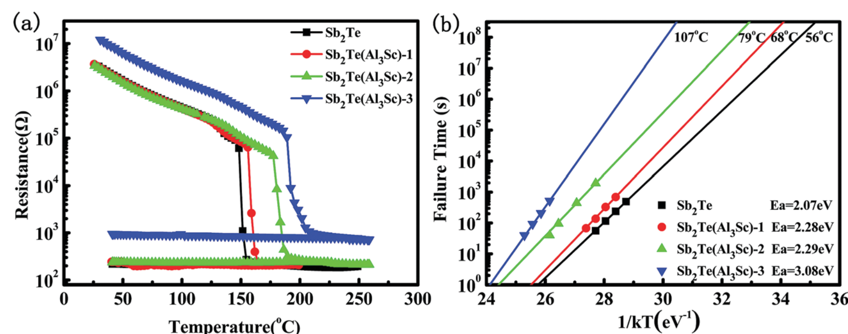

Fig. 1 (a) Temperature-dependence sheet resistance for Al_3Sc-doped Al_3Sc–Sb_2Te films. The heating rate is 20 °C min^{-1}. (b) Arrhenius fitting plots of Al_3Sc-doped Al_3Sc–Sb_2Te films for evaluating data retention and activation energy of crystallization.

 This journal is © The Royal Society of Chemistry 2018

View Article Online

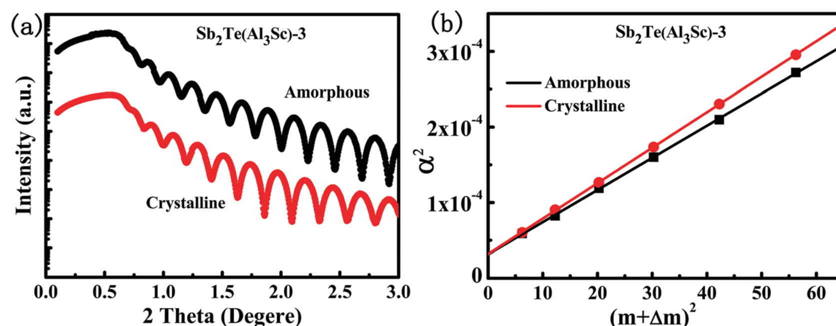

Fig. 2 (a) XRR curves of amorphous and crystalline $Sb_2Te(Al_3Sc)$-3 films. The crystalline $Sb_2Te(Al_3Sc)$-3 film was annealed at 230 °C for 3 min in a N_2 atmosphere. Theta is the angle of incidence X-ray. (b) Bragg fitting curves of amorphous and crystalline $Sb_2Te(Al_3Sc)$-3 films. The symbol m shows the order of reflection indicating each peak in the XRR.

Published on 09 March 2018. Downloaded on 24/04/2018 12:51:46.

and after annealing. m represents the order of reflection, which indicates each peak in the curve. Δm is a constant 1/2 or 0. When the density of the film is larger than the density of the substrate, the value of Δm is 1/2. In contrast, the value is 0. The density of the $Sb_2Te(Al_3Sc)$-3 film is larger than the density of the Si substrate, so Δm should be 1/2 for the $Sb_2Te(Al_3Sc)$-3/Si film.

The fitted dots in Fig. 2(b) are derived from the XRR data. In order to obtain the thickness change, we fit these dots according to the formula[29]

$$\alpha_m^2 = 2\delta + (m + \Delta m)^2 \left(\frac{\lambda}{2t}\right)^2 \quad (1)$$

where α is the radian corresponding to the angle of incidence, δ is the scattering related term and λ is the wavelength of the $Cu_{K\alpha}$ spectral line (0.154 nm) and t is the thickness of the films: it can be calculated from the formula

$$t = \lambda/2\sqrt{k} \quad (2)$$

where k is the slope of the linear fit line. The thickness of $Sb_2Te(Al_3Sc)$-3 is 37.2 nm for the amorphous state, and 35.6 nm for the crystalline state. Therefore, the thickness of the $Sb_2Te(Al_3Sc)$-3 film changes by 4.2%. However, the thickness change of the Sb_2Te film is 5.7%,[30] and the thickness change of the GST film is 6.5%.[31] The thickness change of the $Sb_2Te(Al_3Sc)$-3 film is smaller than those of Sb_2Te and GST films. Smaller changes in the density are desirable for better device performance.

The crystal structures of Sb_2Te and $Sb_2Te(Al_3Sc)$-3 films were analyzed by XRD. As shown in Fig. 3, the Sb_2Te film completely crystallizes into the hexagonal phase of Sb_2Te at an annealing temperature of 230 °C. For Al_3Sc-doped Sb_2Te films, $Sb_2Te(Al_3Sc)$-3 can also be crystallized into a hexagonal Sb_2Te phase at an annealing temperature of 230 °C. The intensities of the (103) and (110) peaks are greatly enhanced, which indicates that the crystallization of these peaks is strongly improved by doping Al_3Sc. According to the Scherrer formula: $D = \dfrac{K\gamma}{B\cos\theta}$, where K is the Scherrer constant (K = 0.89), D is the grain size, B is the full width at half maximum (FWHM) of the diffraction peak of the sample, θ is the diffraction angle, and γ is the X-ray wavelength (0.154056 nm). The exact FWHM values of $Sb_2Te(Al_3Sc)$-3 and Sb_2Te are obtained using jade 6 (a software to analyze the XRD patterns). The FWHM of first three peaks of $Sb_2Te(Al_3Sc)$-3 are 0.292°, 0.487°, 0.322° respectively; and the FWHM of first three peaks of Sb_2Te are 0.185°, 0.393°, and 0.262° respectively. The larger the FWHM, the smaller the grain size. The FWHM of $Sb_2Te(Al_3Sc)$-3 is larger than the FWHM of Sb_2Te, indicating that $Sb_2Te(Al_3Sc)$-3 has a smaller grain size than Sb_2Te.

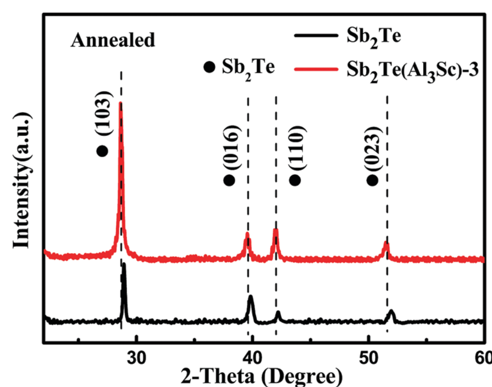

Fig. 3 XRD patterns of Sb_2Te and $Sb_2Te(Al_3Sc)$-3 films annealed at 230 °C for 3 min in a N_2 atmosphere.

As shown in Fig. 4, the morphology and structural features of Sb_2Te and $Sb_2Te(Al_3Sc)$-3 films were analyzed by TEM, HRTEM and SEAD. Comparing Fig. 4(a) with Fig. 4(b), it can be found that the grain size of Sb_2Te is about hundreds of nanometers, while the grain size of $Sb_2Te(Al_3Sc)$-3 is dozens of nanometers, confirming that the FWHM of $Sb_2Te(Al_3Sc)$-3 is larger than that of Sb_2Te. In addition, smaller and uniform crystalline grains of $Sb_2Te(Al_3Sc)$-3 are distributed on the surface, which may be responsible for the reliability of the PCM device. From the HRTEM images of the $Sb_2Te(Al_3Sc)$-3 film in Fig. 4(c), several calculated inter-planar distances indicate that the crystalline material of the $Sb_2Te(Al_3Sc)$-3 film is composed of the hexagonal phase of Sb_2Te. This result can be further proved by comparing the SAED pattern of the $Sb_2Te(Al_3Sc)$-3 film shown in Fig. 4(d). In Fig. 4(d), the corresponding interplanar spacing of the diffraction ring is calculated, and the interplanar spacing is compared with the interplanar distance in the XRD diffraction peak to determine the diffraction crystal plane of the diffractive ring in SAED. The SAED pattern of the

Published on 09 March 2018. Downloaded on 24/04/2018 12:51:46.

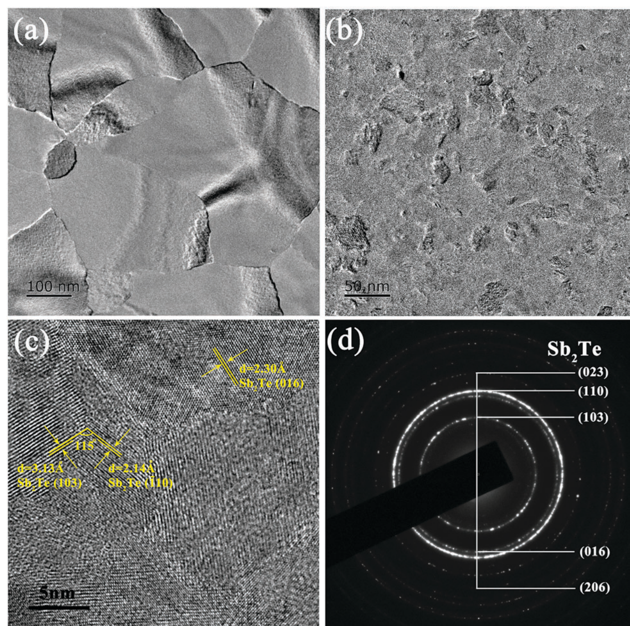

Fig. 4 (a) TEM image for the 230 °C annealed Sb_2Te sample. (b–d) Are TEM, HRTEM, and the SAED images for the 230 °C annealed $Sb_2Te(Al_3Sc)$-3 sample.

$Sb_2Te(Al_3Sc)$-3 film shows that the $Sb_2Te(Al_3Sc)$-3 film is composed of the hexagonal phase of Sb_2Te. Furthermore, the more continuous the rings, the smaller the grain size. And the continuous diffraction rings show that the crystalline structure of the $Sb_2Te(Al_3Sc)$-3 film has a smaller grain size,[32] which helps reduce the residual stress in the bulk of films due to the small probability of grain boundary diffusion or slippage.[33,34] Fig. 5 shows *in situ* heating bright-field TEM images and the corresponding SAED patterns of the $Sb_2Te(Al_3Sc)$-3 film. The images at different temperatures reveal the thermally-induced amorphous-to-hexagonal phase transformation. Fig. 5(a–c) show the amorphous phase of $Sb_2Te(Al_3Sc)$-3, the diffraction patterns are a ring-shaped diffusely scattered halo. While Fig. 5(d–f) show the crystal phase of $Sb_2Te(Al_3Sc)$-3, the diffraction patterns are continuous concentric rings. And it can be found that $Sb_2Te(Al_3Sc)$-3 films crystallize at about 180 °C.

To estimate the electrical performance of the Al_3Sc alloy doped Al_3Sc–Sb_2Te material, PCM devices based on the $Sb_2Te(Al_3Sc)$-3 film were fabricated. Fig. 6(a) shows the typical *R*–*V* characteristic of the $Sb_2Te(Al_3Sc)$-3 based cells. When the pulse width is 10 ns, the voltage required for SET/RESET operation of $Sb_2Te(Al_3Sc)$-3 is only 1.4 V/2.7 V. However, at a 10 ns pulse width, the voltage required for SET/RESET operation of GST is 4.6 V/5.5 V, and the voltage required for SET/RESET operation of $Sc_{0.2}Sb_2Te_3$ is 1.8 V/3 V.[18] When the pulse width is 20 ns, the voltage required for SET/RESET operation of Sb_2Te is 2.8 V/7 V.[30] Therefore, $Sb_2Te(Al_3Sc)$-3 has a lower SET/RESET operation voltage at 10 ns. The energy consumption for RESET operation E_{reset} is estimated by using the equation $E_{reset} = (V_{reset}^2/R_{set}) \times t_{reset}$. The E_{reset} of $Sb_2Te(Al_3Sc)$-3 is about 1.38×10^{-11} J, which is one-seventieth of the E_{reset} of the GST cell (9.7×10^{-10} J).[35] Fig. 6(b) shows that the $Sb_2Te(Al_3Sc)$-3 based PCM device can realize reversible phase transition with a large resistance ratio of about 10^2 and up to 1×10^6 switching cycles were demonstrated. The electrical pulses for SET and RESET operations are 100 ns/2 V and 50 ns/4 V, respectively. While a normal Sb_2Te device only can be stably operated about 4×10^4 cycles. The grain size of Sb_2Te is larger so that it is harder to realize electrical pulse operations and eventually the cell tends to fail.[30] However, doping Al_3Sc can reduce the grain size and improve the endurance characteristics. The uniform distribution of small crystalline grains can be good for enhancing the stability of the practical device.[36] The excellent thermal stability, low power consumption, fast operation speed and good endurance of $Sb_2Te(Al_3Sc)$-3 prove that Al_3Sc alloy doped Al_3Sc–Sb_2Te chalcogenide is a promising candidate for PCM.

Above investigations indicate that the Al_3Sc–Sb_2Te alloy has good thermal stability, low power consumption, and high

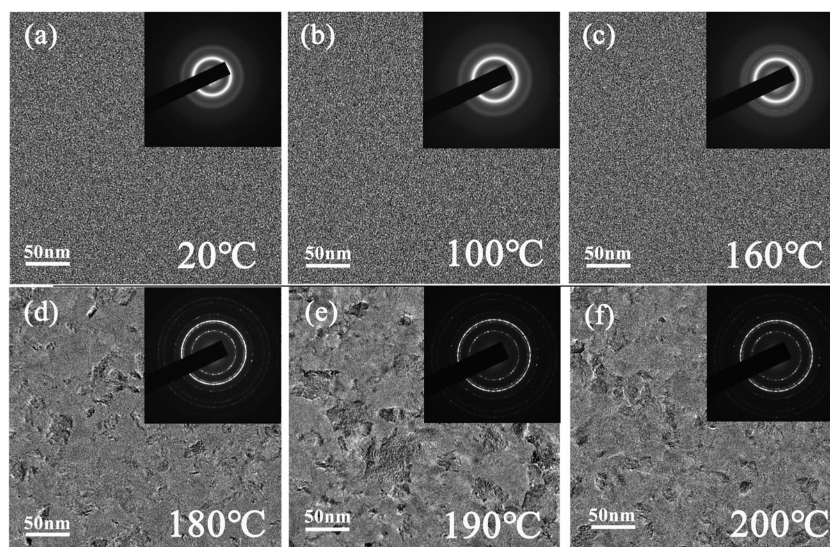

Fig. 5 *In situ* heating bright-field TEM images and the corresponding SAED patterns of the $Sb_2Te(Al_3Sc)$-3 film.

This journal is © The Royal Society of Chemistry 2018

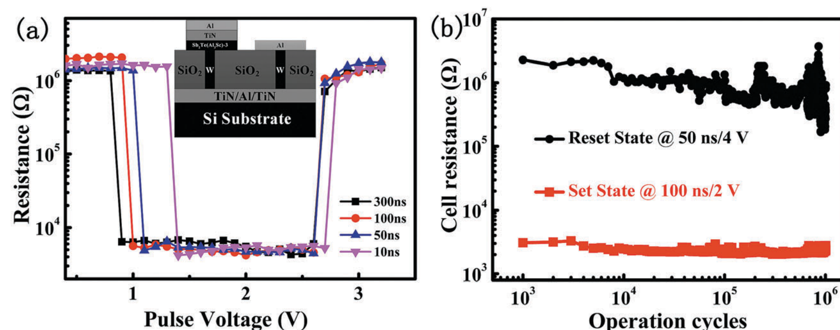

Fig. 6 (a) R–V characteristics of PCM test cell devices fabricated with $Sb_2Te(Al_3Sc)$-3 films. The inset shows the schematic cross-sectional structure of a PCM cell. (b) Endurance characteristics of PCM test cell devices fabricated with $Sb_2Te(Al_3Sc)$-3 films.

Table 1 Formation energy of six binary alloys

	AlSc	AlSb	Al_2Te_3	ScSb	ScTe	Sb_2Te_3
ΔE (eV per atom)	−0.4869	−0.1535	−0.4289	−0.9852	−1.1939	−0.1333
Cell	$a = b = c =$ 3.332 Å $\alpha = \beta = \gamma = 90°$	$a = b = c =$ 6.198 Å $\alpha = \beta = \gamma = 90°$	a = 7.22179 Å b = 12.90218 Å c = 14.36675 Å $\alpha = \gamma = 90°$ $\beta = 89.82339°$	$a = b = c =$ 5.844 Å $\alpha = \beta = \gamma = 90°$	$a = b$ = 4.109 Å c = 6.88745 Å $\alpha = \beta = 90°$ $\gamma = 120°$	$a = b$ = 4.31921 Å c = 29.93174 Å $\alpha = \beta = 90°$ $\gamma = 120°$
Space group	$Pm\bar{3}m$	$F\bar{4}3m$	$P21/c$	$Fm\bar{3}m$	$P63/mmc$	$R\bar{3}m$

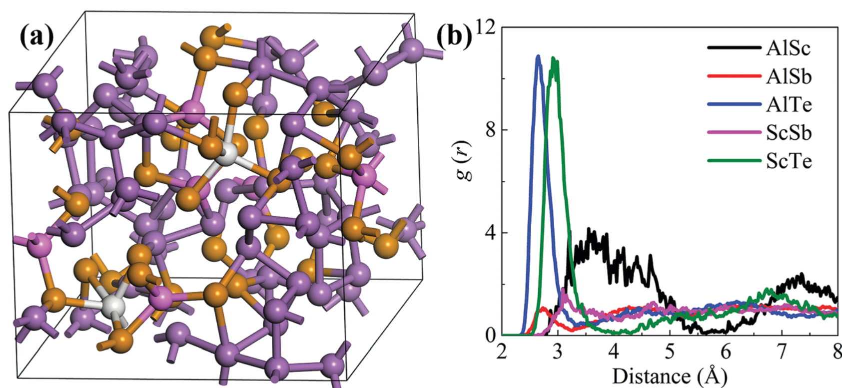

Fig. 7 The structure features of Al_3Sc–Sb_2Te at 800 K. (a) A typical amorphous structure. (b) The PDFs of Al–Sc, Al–Sb, Al–Te, Sc–Sb, and Sc–Te pairs.

operation speed. To further study the bonding characteristics of the Al_3Sc–Sb_2Te alloy film, the formation energy of binary alloys was calculated, as shown in Table 1, in which the most stable alloys or elementary substances are chosen. The formation energy of the absolute value is large as doping elements mix with Sb or Te elements, such as about −1 eV per atom for the Sc element, while Sb_2Te_3 has the smallest value. In addition, Al and Sc elements have larger formation energy with Te than that with Sb. These features determine stable local patterns in the amorphous state in which both Al and Sc elements prefer contacting with Te atoms.

In order to obtain the amorphous structure, we carry out an AIMD simulation. Fig. 7(a) shows a typical structure during the simulation. In the figure, we found that Al and Sc atoms are always bonding with Te atoms, in line with the above formation-energy analysis. In the figure, the coordinate numbers (CNs) for Al and Sc atoms are four and five, respectively. Fig. 7(b) shows the pair distribution functions (PDFs) of five pairs for the time average during 40 ps. It strongly exhibits two main [$AlTe_4$] and [$ScTe_5$] patterns in the amorphous structures due to the highest first peaks of Al–Te and Sc–Te pairs. These stable patterns can stabilize the glassy state. The stable [$ScTe_5$] pattern of CN close to six can be considered as a nucleating centre to accelerate crystallization.[18] These make the Al_3Sc–Sb_2Te alloy film not only highly thermally stable but also maintains fast transition speed. These performances show that the Al_3Sc–Sb_2Te phase change material would be a promising candidate for PCM.

4. Conclusion

In summary, high performance Al_3Sc alloy doped Al_3Sc–Sb_2Te materials are proposed and investigated. The crystallization temperature of 189 °C and an estimated 10-year data retention temperature of 107 °C indicate that the Al_3Sc–Sb_2Te material has much better thermal stability than conventional GST and

Published on 09 March 2018. Downloaded on 24/04/2018 12:51:46.

Published on 09 March 2018. Downloaded on 24/04/2018 12:51:46.

Sc-doped $Sc_{0.2}Sb_2Te_3$ materials. The $Al_3Sc–Sb_2Te$ material has a refined grain size and a small density change upon phase transition. The $Al_3Sc–Sb_2Te$ based device shows excellent reversible SET–RESET properties with a suitable operation window and a low power consumption of 1.38×10^{-11} J. The endurance of 1×10^6 cycles with a large resistance ratio of about 10^2 was demonstrated. Our calculations reveal that Al and Sc atoms prefer bonding with Te atoms. These stable local patterns can stabilize glassy states. The excellent performances of Al_3Sc alloy doped $Al_3Sc–Sb_2Te$ chalcogenide make it a promising material for PCM application. A further study needs to be performed on whether the $Al_3Sc–Sb_2Te$ material has better performance at sub-nanosecond pulse.

Conflicts of interest

There are no conflicts to declare.

Acknowledgements

This work was supported by the National Key Research and Development Program of China (2017YFB0701703, 2017YFB0206101), Strategic Priority Research Program of Chinese Academy of Sciences (XDA09020402), and National Natural Science Foundation of China (61076121, 11475043).

Notes and references

1 M. Wuttig and N. Yamada, *Nat. Mater.*, 2007, **6**, 824.
2 M. Xu, Y. Q. Cheng, L. Wang, H. W. Sheng, Y. Meng, W. G. Yang, X. D. Han and E. Ma, *Proc. Natl. Acad. Sci. U. S. A.*, 2012, **109**, E1055–E1062.
3 M. Xu, Y. Q. Cheng, H. W. Sheng and E. Ma, *Phys. Rev. Lett.*, 2009, **103**, 195502.
4 G. Atwood, *Science*, 2008, **321**, 210–211.
5 S. Raoux, W. Wełnic and D. Ielmini, *Chem. Rev.*, 2010, **110**, 240–267.
6 Z. Li, C. Si, J. Zhou, H. B. Xu and Z. M. Sun, *ACS Appl. Mater. Interfaces*, 2016, **8**, 26126–26134.
7 J. Kalikka, X. Zhou, E. Dilcher, S. Wall, J. Li and R. E. Simpson, *Nat. Commun.*, 2016, **7**, 11983.
8 S. R. Ovshinsky, *Phys. Rev. Lett.*, 1968, **21**, 1450–1453.
9 M. Xu, Z. H. Yu, L. Wang, R. Mazzarello and M. Wuttig, *Adv. Electron. Mater.*, 2015, **1**, 7.
10 Z. M. Sun, J. Zhou, H. J. Shin, A. Blomqvist and R. Ahuja, *Appl. Phys. Lett.*, 2008, **93**, 3.
11 Z. Sun, J. Zhou, Y. Pan, Z. Song, H.-K. Mao and R. Ahuja, *Proc. Natl. Acad. Sci. U. S. A.*, 2011, **108**, 10410–10414.
12 B. Sa, J. Zhou, Z. Sun, J. Tominaga and R. Ahuja, *Phys. Rev. Lett.*, 2012, **109**, 096802.
13 Z. Sun, J. Zhou, A. Blomqvist, B. Johansson and R. Ahuja, *Phys. Rev. Lett.*, 2009, **102**, 075504.
14 Z. M. Sun, J. Zhou, A. Blomqvist, B. Johansson and R. Ahuja, *Appl. Phys. Lett.*, 2008, **93**, 3.
15 Z. M. Sun, J. Zhou, H. K. Mao and R. Ahuja, *Proc. Natl. Acad. Sci. U. S. A.*, 2012, **109**, 5948–5952.
16 M. Zhu, L. Wu, F. Rao, Z. Song, K. Ren, X. Ji, S. Song, D. Yao and S. Feng, *Appl. Phys. Lett.*, 2014, **104**, 053119.
17 M. Zhu, M. Xia, F. Rao, X. Li, L. Wu, X. Ji, S. Lv, Z. Song, S. Feng, H. Sun and S. Zhang, *Nat. Commun.*, 2014, **5**, 4086.
18 F. Rao, K. Y. Ding, Y. X. Zhou, Y. H. Zheng, M. J. Xia, S. L. Lv, Z. T. Song, S. L. Feng, I. Ronneberger, R. Mazzarello, W. Zhang and E. Ma, *Science*, 2017, **358**, 1423–1426.
19 M. Zhu, L. C. Wu, Z. T. Song, F. Rao, D. L. Cai, C. Peng, X. L. Zhou, K. Ren, S. N. Song, B. Liu and S. L. Feng, *Appl. Phys. Lett.*, 2012, **100**, 4.
20 J. B. Mann, T. L. Meek, E. T. Knight, J. F. Capitani and L. C. Allen, *J. Am. Chem. Soc.*, 2000, **122**, 5132–5137.
21 J. B. Mann, T. L. Meek and L. C. Allen, *J. Am. Chem. Soc.*, 2000, **122**, 2780–2783.
22 G. Kresse and J. Furthmuller, *Phys. Rev. B: Condens. Matter Mater. Phys.*, 1996, **54**, 11169–11186.
23 G. Kresse and J. Furthmuller, *Comput. Mater. Sci.*, 1996, **6**, 15–50.
24 G. Kresse and J. Hafner, *Phys. Rev. B: Condens. Matter Mater. Phys.*, 1994, **49**, 14251–14269.
25 G. Kresse and J. Hafner, *Phys. Rev. B: Condens. Matter Mater. Phys.*, 1993, **47**, 558–561.
26 P. E. Blochl, *Phys. Rev. B: Condens. Matter Mater. Phys.*, 1994, **50**, 17953–17979.
27 J. P. Perdew, K. Burke and M. Ernzerhof, *Phys. Rev. Lett.*, 1996, **77**, 3865–3868.
28 H. R. L. Martijn, P. Liesbeth van, S. Mark van, A. J. J. Ben and C. N. R. Jan, *Jpn. J. Appl. Phys.*, 2003, **42**, 863.
29 Q. Zhang, S. F. Yoon, Rusli, J. Ahn, H. Yang and D. Bahr, *J. Appl. Phys.*, 1999, **86**, 289–296.
30 G. Liu, L. Wu, M. Zhu, Z. Song, F. Rao, S. Song and Y. Cheng, *Solid-State Electron.*, 2017, **135**, 31–36.
31 W. K. Njoroge, H. W. Woltgens and M. Wuttig, *J. Vac. Sci. Technol., A*, 2002, **20**, 230–233.
32 Y. Cheng, Z. Song, Y. Gu, S. Song, F. Rao, L. Wu, B. Liu and S. Feng, *Appl. Phys. Lett.*, 2011, **99**, 261914.
33 R. Feng, S. Zhitang, R. Kun, Z. Xilin, C. Yan, W. Liangcai and L. Bo, *Nanotechnology*, 2011, **22**, 145702.
34 X. Zhou, J. Kalikka, X. Ji, L. Wu, Z. Song and R. E. Simpson, *Adv. Mater.*, 2016, **28**, 3007–3016.
35 Y. Hu, X. Zhu, H. Zou, J. Zhang, L. Yuan, J. Xue, Y. Sui, W. Wu, S. Song and Z. Song, *Appl. Phys. Lett.*, 2016, **108**, 223103.
36 C. Peng, Z. Song, F. Rao, L. Wu, M. Zhu, H. Song, B. Liu, X. Zhou, D. Yao, P. Yang and J. Chu, *Appl. Phys. Lett.*, 2011, **99**, 043105.

This journal is © The Royal Society of Chemistry 2018